

Study on Risk Analysis of Large-scale Landslide

Teng-Chieh HSU¹, Yuan-Jung TSAI^{2*}, Chjeng-Lun SHIEH³ and Jen-Yuen CHENG⁴

¹ Graduate student, Department of Hydraulic and Ocean Engineering, National Cheng Kung University, Taiwan

² Researcher, Disaster Prevention Research Center, National Cheng Kung University, Taiwan

³ Director, Disaster Prevention Research Center, National Cheng Kung University, Taiwan

⁴ Engineer, Southern Region Water Resources Office, WRA, MOEA, Taiwan

*Corresponding author. E-mail: rongtsai@dprc.ncku.edu.tw

With the implement of mitigation work of large-scale landslide, hundreds of potential large-scale landslide areas were identified in Taiwan since 2010. The topographical features, geological conditions and situation of property and residents were used to evaluate the risk for each potential large-scale landslide in the first stage. Therefore, a lot of countermeasures and monitoring systems were setup to reduce the risk of potential large-scale landslide. However, the approach of risk assessment in the first stage did not consider risk distribution in a regional area, so that the effect of mitigation work and land-use management cannot be estimated. In this study, we present a risk assessment approach to evaluate the risk of large-scale landslide and the effect of the mitigation work.

The risk is the probability of potential loss. In this study, we define the risk is the function of hazard, exposure and vulnerability. Hazard is considering the deposition depth and movement velocity. Exposure is considering the land use (building, road, agricultural land, forest), which is exposed in the hazard area. Vulnerability is considering the relationship between land use, hazard, and loss curve. Furthermore, this approach considers the effect of mitigation work such as land-use management and sabo work. The result shows that, the potential loss can be well quantify with the approach. Furthermore, the effect of the mitigation work, such as land use managements and sabo works, can be also well described in this approach.

Key words: large-scale landslide; risk analysis; landslide disaster

1. INTRODUCTION

Large-scale landslide disasters have caused severe damages in Taiwan in the past years. As a result, it is an urgent task for the government and the research communities to start series mitigation work to reduce the loss of the disaster. With the implement of mitigation work of large-scale landslide, hundreds of potential large-scale landslide areas were identified in Taiwan since 2010. The topographical features, geological conditions and situation of property and residents were used to evaluate the risk for each potential large-scale landslide in the first stage.

Therefore, lots countermeasures and monitoring systems were setup to reduce the risk of potential large-scale landslide. However, the approach of risk assessment in the first stage was setup to identify the risk from hundreds of potential large-scale landslide areas with topography, geology and number of buildings. The current method could only prioritize the sequence of countermeasure based on the risk of each potential large-scale landslide, the

post effectiveness assessment of countermeasures, is dismissed.

The main propose of this research, in terms of the response action in the disaster management, is to study the risk of large-scale landslide, and to provide the foundation for mitigation work. In this study, we present a new risk assessment approach, which can evaluate the risk for each potential large-scale landslide and can identify risk map in a regional area. Moreover, the presented approach considers the effect of mitigation work.

2. METHODS

2.1 Risk assessment

In this study, risk is defined as the probability of potential loss. The risk index approach, which can help to understand the contribution of hazard, vulnerability and exposure to overall risk is used to analyze the risk of large-scale landslide. The risk is the function of hazard, exposure and vulnerability. Risk is expressed as:

$$R = f(H, E, V) \quad (1)$$

R is risk of large-scale landslide, H is hazard, E is exposure, V is vulnerability. **Fig.1** show the concept of the risk mapping in this study. Consequently, the risk mapping is processed by GIS tools. First drawing the 2m x 2m square grid meshes on the case study areas. In this size of mesh, the damage of buildings could be well evaluated in spatial distribution.

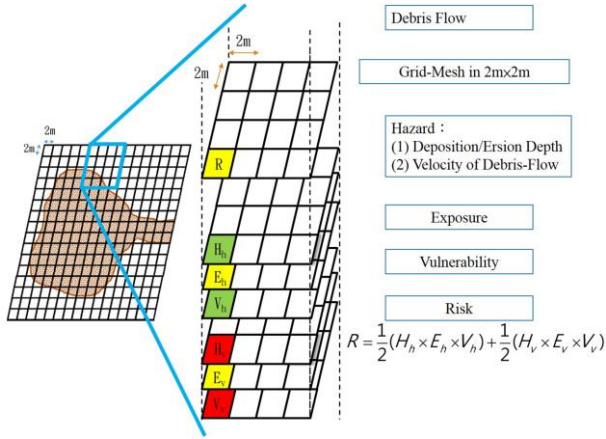


Fig1. Concept of risk mapping

The hazards are evaluated with the velocity of landslide movement and depth of landslide deposition, which are evaluated by numerical. Because of high water content of landslide mass, the landslide movement is considered as a continuous solid-liquid phase flow. This research simulated the process of landslide by the numerical model, which was developed by Egashira et al. (1997) and was modified by Miyamoto (2002).

The exposures are evaluated with four kinds of land use, such as building, road, agricultural land and forest.

The vulnerability was evaluated with the loss curve of four kinds of land use and the population composition, which is considering the distribution of population age. Consequently, the risk mapping is processed by GIS tools.

Therefore, we can evaluation the hazards, exposures, vulnerability of each grid mesh with Eq. (1) to evaluate the large-scale landslide risk of all each grid mesh. Finally, we can map the risk distribution in a regional area.

2.2 Hazard assessment

We considered the landslide movement as a continuous solid-liquid phase flow. This model assumes that (1) the movement of landslide mass can be considered as the movement of solid-liquid mixture at constant solid concentration on a fixed bed and (2) the quasi-static inter-granular friction

stress dominates the flow characteristics. This model uses kinematic energy balance in shear flow to simulate the rheology of the solid-liquid mixture of the landslide. During the movement of landslide mass, the concentration of solid particles is assumed unchanged, and the quasi-static inter-granular friction stress is not balanced with the external shear stress at the bed. Based on the evaluation of the static inter-granular friction stress, the dynamics of the landslide mass can be determined.

In the model, the friction angle is constant in the model, which the friction is changing with the velocity of the landslide mass. The governing equations include continuity equation and momentum equation:

Continuity equation

$$\frac{\partial h}{\partial t} + \nabla g \mathbf{M} = 0 \quad (2)$$

Momentum equation

$$\frac{\partial \mathbf{M}}{\partial t} + \beta (\mathbf{M} u^t) \nabla = -gh \nabla H - \frac{\mathbf{T}}{\rho_m} \quad (3)$$

where h is landslide thickness, \mathbf{M} is the flux vector, β is the coefficient of momentum, and u is depth-averaged velocity. Superscript t of \mathbf{u} means transverse of the corresponding vector or matrix, that is, \mathbf{u}^t is the transverse vector of \mathbf{u} , g is gravity acceleration, H is the surface level of the landslide, and the lateral earth pressure within the debris mass is assumed to be unity. \mathbf{T} is the shear stress acting on the slip surface, and ρ_m is the mass density of a hyper-concentrated sediment-water mixture. The density is determined as

$$\rho_m = c\sigma + (1 - c)\rho \quad (4)$$

where σ is the mass density of solid phase, ρ is the mass density of liquid phase, and c is the volumetric concentration of solid phase, and ∇ is defined as $\nabla = \partial/\partial x_i + \partial/\partial y_j$, in which i and j are base vectors of Cartesian coordinates. In Eq.(2), deposition and erosion are assumed not to occur during the landslide movement so the right side of the equation is set to zero. Egashira et al. (1997) established the shear stress \mathbf{T} based on energy consideration, $\Phi = (\partial u / \partial x_j) \mathbf{T}$. In this equation, the shear stress \mathbf{T} is obtained from the energy dissipation of particle and stream flow Φ . The shear stress is then introduced into the momentum equation. We assumed that shear stress \mathbf{T} acts on the slip surface and can be expressed as:

$$\mathbf{T} = \mathbf{T}_s + \mathbf{T}_d + \mathbf{T}_f \quad (5)$$

where T_s is the shear stress due to static inter-granular contacts, T_d is the shear stress due to particle-to-particle collisions, and T_f is the shear stress due interstitial liquid phase turbulent and those can be expressed as:

$$\mathbf{T}_s = \alpha C(\sigma - \eta\rho)gh\cos\theta\tan\phi_s \frac{\mathbf{u}}{|\mathbf{u}|}, \quad (6)$$

$$\alpha = \left(\frac{C}{C_*}\right)^{1/5} \quad (7)$$

$$\mathbf{T}_d = \frac{25}{4}k_g\sigma(1 - e^2)C^{1/3}\left(\frac{d}{h}\right)\mathbf{u}|\mathbf{u}| \quad (8)$$

$$\mathbf{T}_f = \frac{25}{4}k_f\sigma(1 - c)^{5/3}C^{2/3}\left(\frac{d}{h}\right)\mathbf{u}|\mathbf{u}| \quad (9)$$

where ϕ_s is the friction angle, e is the restitution coefficient, c_* obtained from the field investigation are the concentrations of the solid phase in volume in the flow and at a packed state, d is the diameter of particles of the solid phase, k_g and k_f are constants ($k_g=0.0828$ and $k_f=0.16$ to 0.25), θ is the gradient of the slip surface, and $\eta=0.808$ is the coefficient of the effect of buoyancy and takes a value from 0 to 1. In this study, η is suggested by Miyamoto (2002). T_s and T_d will change according to the speed of the sediment movement. When the sediment is moving slow, T_s has larger impact than T_d . Otherwise, it will be the other way around. The internal friction angle is constant. The static inter-granular contact T_s is updated automatically with the movement.

The dynamics of landslide mass is determined using the revised momentum equation. The revised momentum equation can be written as:

$$\mathbf{M}^{n+1} = \mathbf{M}^n - \left[\beta(\mathbf{M}^n \mathbf{u}^{in})\nabla + (\mathbf{T}_s^n + \mathbf{T}_d^n + \mathbf{T}_f^n) / \rho_m + g\mathbf{h}^n \nabla H^n \right] \Delta t \quad (9)$$

where n denotes the present time step and $n+1$ denotes the next time step. As shown in the equation, the dynamics is determined not by the friction but the value of \mathbf{M} . When $\mathbf{M}>0$, the mass is in motion. On the other hand, the mass is not in motion when $\mathbf{M}<0$. For more details, please refer to Miyamoto (2002).

There are two limitations for the proposed model. First, the erosion of the slide surface due to the movement of landslide mass is not considered in the model. Second, the water content of landslide material is constant. In this case, the soil mass is saturated during the landslide event.

The hazards of velocity of landslide movement and depth of landslide deposition, which are evaluated by numerical model could be set with **Table 1**.

Table1 Hazard values base on numerical result

velocity of landslide (m/s)	H_v	depth of landslide deposition(m)	H_h
0.5~1	0.2	1.5~2.5	0.2
1~2	0.4	2.5~6	0.4
2~3	0.6	6~8	0.6
3~5	0.8	8~12	0.8
>5	1	>12	1

2.3 Exposure assessment

In this study, we quantified exposure based on the depth of landslide deposits and landslide velocity, which were represented as E_h and E_v , respectively.

These two exposure factors were assessed as follows. Each grid cell was assigned a deposition depth value that reflected the final deposition condition in the earth covered by that cell. If deposition becomes hazardous once its depth exceeds 0.5 m, then E_h equals 1 if the depth of landslide deposits is greater than 0.5 m; otherwise E_h equals 0, as shown in **Table 2**.

Grid cells were assigned landslide velocity values that matched the maximum velocity of landslide material passing through them. If landslide velocity becomes hazardous once it exceeds 1.5 m/s, then E_v equals 1 if landslide velocity is greater than 1.5 m/s; otherwise E_v equals 0, as shown in **Table 3**.

Table 2 Exposure values based on depth of landslide deposits

Depth-based exposure	Value
depth of deposits>0.5m	1
depth of deposits<0.5m	0

Table 3 Exposure values based on landslide velocity

Velocity-based exposure	Value
landslide velocity >1.5 m/s	1
landslide velocity <1.5 m/s	0

2.4 Vulnerability assessment

In this study, we quantified vulnerability according to the depth of landslide deposits, landslide velocity, and the village dependency ratio. These factors were represented as V_h , V_v , and I_{DR} , respectively.

V_h and V_v were determined for a variety of land-cover types (buildings, roads, agriculture, and forests). Specifically, V_{hh} , V_{hr} , V_{ha} , and V_{hf} respectively quantify how depth of landslide deposits affect the vulnerability of building, road, agriculture, and forest land-cover types. V_{vh} , V_{vr} , V_{va} , and V_{vf} respectively quantify how landslide velocity affects the vulnerability of building, road, agriculture, and forest land-cover types. Note that the first letter of the subscripts denotes the hazard

type (depth of landslide deposits or landslide velocity), and the second letter of the subscript denotes the land-cover type (building, road, agriculture, or forest). In other words:

$V_{\alpha\beta}$: represents the vulnerability of land-cover type β exposed to hazard α , where α : depth of landslide deposits (h) or landslide velocity (v); β : building (h), road (r), agriculture (a), or forest (f).

The formulas used to combine the various $V_{\alpha\beta}$ values were as follows (Eqs. 10 and 11):

$$V_h = (0.4V_{hh} + 0.3V_{hr} + 0.2V_{ha} + 0.1V_{hf}) \cdot I_{DR} \quad (10)$$

$$V_v = (0.4V_{vh} + 0.3V_{vr} + 0.2V_{va} + 0.1V_{vf}) \cdot I_{DR} \quad (11)$$

The partial vulnerability score assigned to each land-cover type was weighted differently, according to the monetary value associated with each land-cover type. In other words, land-cover types with greater monetary value were weighted more highly in the calculation of vulnerability scores.

Below, we explain the analytical methods used to determine (1) vulnerability to depth of landscape deposits and (2) vulnerability to landslide velocity in detail:

Vulnerability of the building land-cover type to depth of landslide deposits, V_{hh} : We referred to the building loss ratio curve used by Lo et al. (2012) to assess the vulnerability of structures located in mountainous areas of Taiwan (**Fig.2**). By substituting the upper limit of values which quantify the depth of landslide deposits in each interval into Eq. (12), we can derive the vulnerability of land used for buildings (**Table 3**).

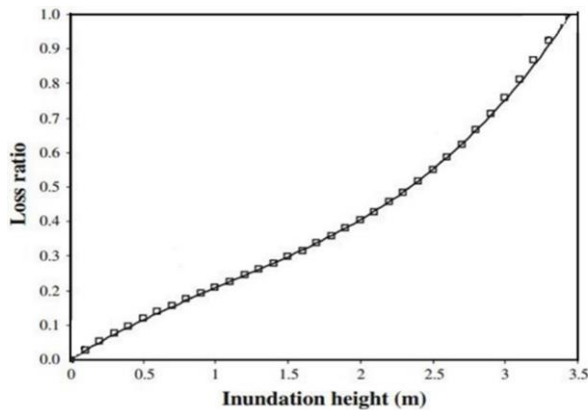


Fig 2. Loss ratio curve at different inundation depths (Lo et al. 2012)

$$V_{build}(h) = \begin{cases} 0.0266h^3 - 0.2663h & \text{if } 0 \leq h < 3 \\ 1 & \text{if } h \geq 3 \end{cases} \quad (12)$$

Vulnerability of the road land-cover type to depth of landslide deposits, V_{hr} : We posit that the primary

expenses related to road damage following a landslide are those incurred clearing and removing landslide deposits. Therefore, these expenses are proportional to deposit volume. All grids cells in this study measured $2m \times 2m$. Therefore, the vulnerability of the road land-cover type is proportional to the depth of landslide deposits. When the depth of landslide deposits is greater than 5 m, then $V_{hr}=1$; when it is less than 0.5 m, then $V_{hr}=0$. **Table 3** presents the relationship between vulnerability to financial loss and depth of landslide deposits.

Vulnerability of the agriculture land-cover type to depth of landslide deposits, V_{ha} : Agricultural crops can be easily damaged from landslides. Crops completely lose economic value when buried under landslide debris, so we assumed that $V_{ha}=1$ if the depth of landslide deposits was greater than 0.5 m.

Vulnerability of the forest land-cover type to depth of landslide deposits, V_{hf} : Broad-leaved trees are the primary type of commercially valuable wood in forests. According to Design and Technique Specifications for Greenery of Site, large broad-leaved trees are defined as trees whose height exceeds 10 m at maturity. For trees on forest land that are 10 m in height; losses are incurred when the depth of landslide deposits reaches 1/4 of tree height, and destruction occurs when landslide deposition depth reaches 1/2 of tree height (**Table 3**).

Vulnerability of the building land-cover type to landslide velocity, V_{vh} : We assumed that damage to buildings begins to occur when landslide velocity reaches 2.5 m/s. At this speed, financial losses are minor (approximately 10% of total possible loss). In contrast, a landslide velocity greater than 12 m/s results in 100% losses. Percent loss values that occur at landslide velocities between 2.5 m/s and 12 m/s were derived using linear interpolation. The relationship between vulnerability to financial loss and landslide velocity is presented in **Table 4**.

Vulnerability of the road land-cover type to landslide velocity, V_{vr} : We assumed that the vulnerability of the road land-cover type to landslide velocity is equal to that of the building land-cover type (**Table 4**).

Vulnerability of the agriculture land-cover type to landslide velocity, V_{va} : We assumed that landslide velocities between 1.5 m/s and 2.5 m/s result in the loss of 50% of crops and that velocities greater than 2.5 m/s cause 100% of crops to be lost (**Table 4**).

Vulnerability of the forest land-cover type to landslide velocity, V_{vf} : We assumed that landslide velocities between 1.5 m/s and 2.5 m/s result in 25% of forest land being lost and that velocities between

8 m/s and 12 m/s result in 100% of forest land being lost. Losses that occur at velocities between 2.5 m/s and 12 m/s were derived using linear interpolation. This relationship is presented in **Table 4**.

This index I_{DR} describes the ability of a village to respond to large-scale landslide disasters according to the age structure of the population. Children and the elderly tend to have poorer mobility than do individuals in other age groups. These individuals are therefore less able to flee from disasters. Therefore, the dependency ratio of a village can be defined as the ratio of children and elderly individuals to the total population, as shown in Eq. 13. A higher I_{DR} indicates that age structure makes the village more vulnerable in the face of a disaster.

$$I_{DR} = (\text{Number of children and elderly}) / (\text{Total population}) \quad (13)$$

Table 3 vulnerability corresponding to depth of landslide deposits

Z(m)	V_{hh}	V_{hr}	V_{ha}	V_{hf}
0~0.5	0	0	0	0
0.5~1	0.21	0.15	1	0
1~2	0.41	0.3	1	0
2~3	0.75	0.5	1	0.33
3~5	1	0.8	1	0.66
>5	1	1	1	1

Table 4 vulnerability corresponding to landslide velocity

V_s (m/s)	V_{vh}	V_{vr}	V_{va}	V_{vf}
0~1.5	0	0	0	0
1.5~2.5	0	0	0.5	0.25
2.5~6	0.1	0.1	1	0.5
6~8	0.4	0.4	1	0.75
8~12	0.7	0.7	1	1
>12	1	1	1	1

3. STUDY AREA

Typhoon Morakot, a medium-strength typhoon, invaded Taiwan from August 5 to 10, 2009, and brought with extremely high intensity and accumulative rainfall. The abnormal heavy rainfall influenced southern and eastern Taiwan. In this research, the risk map of Xinkai landslides, which was triggered by Typhoon Morakot, was evaluated with the presented risk assessment approach.

The Xinkai landslide took place in Xinfu Village, located in the Liouguei District of Kaohsiung City (**Fig.3**). According to the major landslide disaster report provided by the Soil and Water Conservation Bureau, this large-scale landslide occurred on the upstream slopes of a wild stream, behind Xinkai Village, forming a debris flow that caused 38 deaths and damaged 38 buildings.

The Xinkai landslide was located upstream of the potential debris flow torrent known as Kaohsiung DF078. The area of this watershed is approximately 52 ha, and the elevation range 400m to 1100m. In 2009, Xinkai village had a population of 1,711 people, and its dependency ratio was 0.3007.



Fig 3. The aerial photo after typhoon Morakot

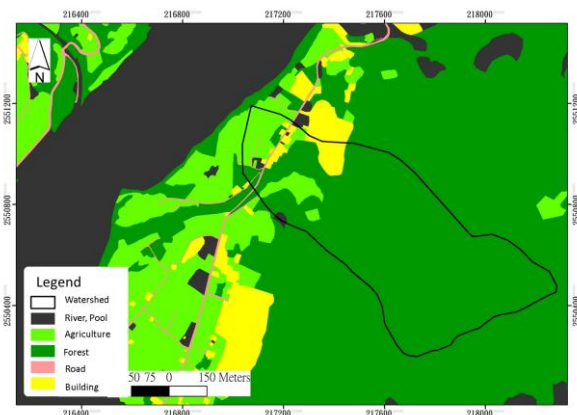


Fig 4. Land cover in Xinkai in 2009

4. RESULT AND DISCUSSION

4.1 Result of Xinkai Village

(a) Result of Hazard assessment

Fig.5 and **Fig.6** present hazard area of the Xinkai landslide. The primary hazard was depth of landslide deposits depth. In this study, grid cells were assigned values that corresponding to the maximum velocity that was reached during the Xinkai landslide. Therefore, the vulnerability score assigned to most of these grid cells was 1. Only a

few cells at the edge of the deposition zone received a vulnerability score of less than 1 for landslide velocity. Conversely, the depth of landslide deposits gradually decreased from the apex of the alluvial fans to the outer edges. As shown in **Fig. 5**, the vulnerability score for depth of landslide deposits for most of the buildings in Xinkai Village ranged from 0.8 to 1.

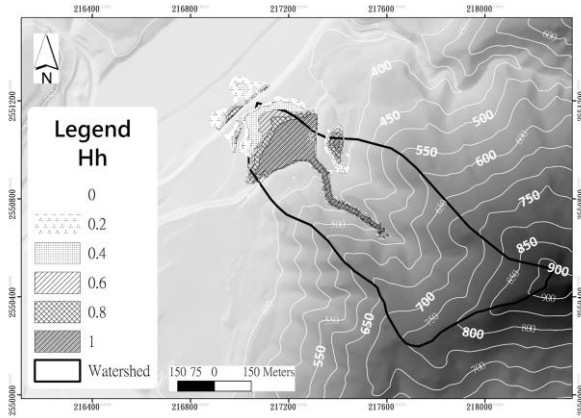


Fig 5. Hazard from landslide deposition depth

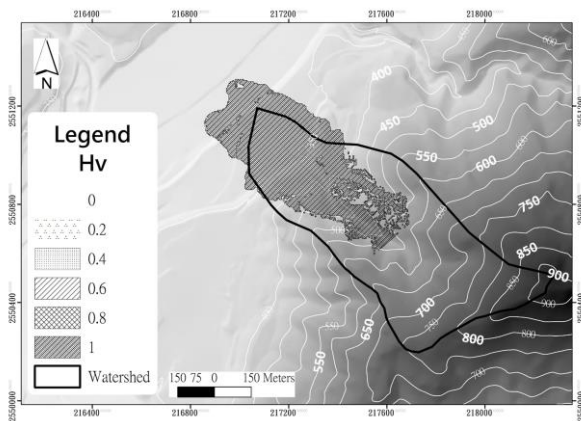


Fig 6. Hazard from landslide velocity

(b) Result of Exposure assessment

The exposure assessment of the Xinkai landslide were shown in **Fig.7** and **Fig.8**. The extent of exposure due to landslide velocity was greater than the extent of exposure due to depth of landslide deposits. This is because, in Eq. 12, we adopted values which corresponded to the maximum velocity that was reached during the landslide. The depth of landslide deposits merely reflects the outcome of the landslide. While the sliding debris of the landslide passed through many grid cells, it was not necessarily deposited there. In other words, the extent of exposure due to landslide velocity equals the extent of the transportation zone plus the extent of the deposition zone, whereas the deposition zone accounts for most of the extent of exposure that results from the depth of landslide deposits.

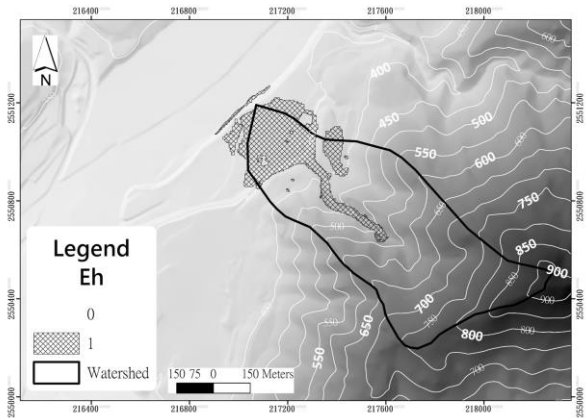


Fig 7. Exposure from landslide deposition depth

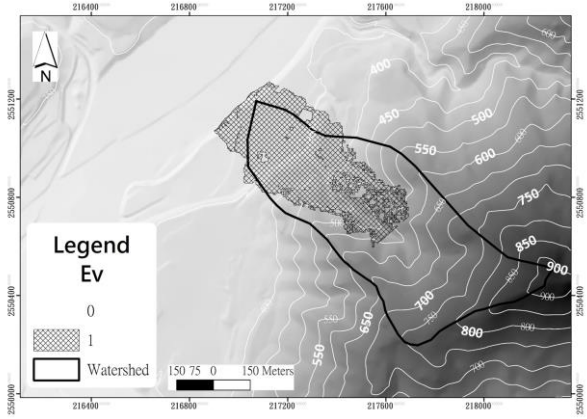


Fig 8. Exposure from landslide velocity

(c) Result of Vulnerability assessment

The vulnerability assessment of Xinkai landslide was shown in **Fig.9** and **Fig.10**. To effectively differentiate the degree of vulnerability of each land-cover type, the weights were set as 0.4, 0.3, 0.2, and 0.1 for buildings, roads, agriculture, and forest, respectively (i.e. buildings have the highest monetary value and forested land has the lowest monetary value). The grid mesh in this study was segmented into 2m×2m square cells. If the land in each grid can only contain a single cover type, the maximum vulnerability value in this study was $V=0.4I_{DR}$, and the minimum vulnerability value was $V=0$.

The building was most vulnerable to landslides. Landslide deposits became shallower further away from the mouth of the valley, whereas landslide velocity did not show much variation. Thus, according to the vulnerability analysis that was performed for depth of landslide deposits, roads on the outer edges of the alluvial fan have moderate vulnerability, while the vulnerability analysis for landslide velocity indicates that roads have high vulnerability.

In **Fig.10** show that the landslide velocity of the

area is very high so that the vulnerability from landslide velocity; on the other hand, some area of oval in Fig.9 is no color means that the landslide debris passed this area but was not deposited there.

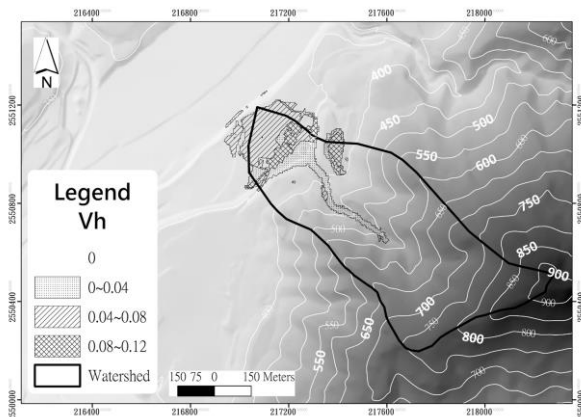


Fig 9. Vulnerability from landslide deposition depth

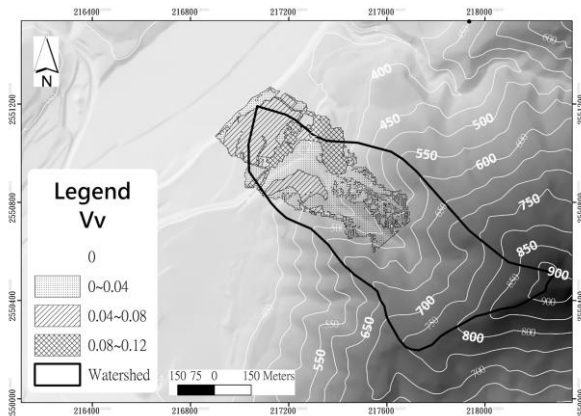


Fig 10. Vulnerability from landslide velocity

(d) Result of Risk assessment

The map of large-scale risk for the Xinkai landslide (Fig.11) reveals that most of the high-risk areas occur on the building land-cover type. This is due to greater hazard, exposure, and vulnerability scores that characterize this land-cover type.

The risk was lower in the transportation zone for two reasons. (1) There were no important protected targets in the transportation zone as most of it was forest land. (2) There were no landslide deposits in grid cells which corresponded to the transportation zone; therefore, the hazard from depth of landslide deposits was 0, which lowered the overall risk. The risk was also lower on the outer edges of the alluvial fan due to shallower landslide deposits, lower landslide velocity, and the fact that most of these areas were forested. Therefore, even with the same degree of exposure, areas with lower hazard and vulnerability scores are at lower risk.

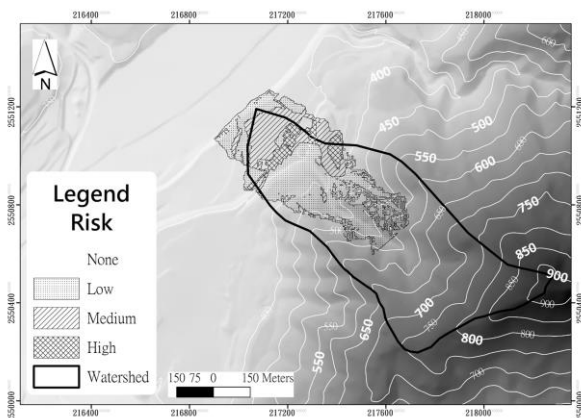


Fig 11. Risk map of Xinkai

4.2 Effect of land use management

Fig.4 shows the land-use adjacent to Xinkai Village before typhoon Morakot. The result of risk mapping before typhoon Morakot (Fig.11) is verified by disaster during the event (Fig.3), leaving 38 dead and destroying 38 building, which located at high risk level area of assessment result. In addition, this research also discusses the relationship between land-use management and risk map (Fig.12, Fig.13).

Comparing Fig.11 with Fig. 13, we find there are some differences. For instance, the high and medium risk level were reduced to no risk due to most residents moved out after sediment disaster in 2009, thus the land-use was change from building and farm to barren land. The effect of sabo works is considering in the presented approach as well (Fig.14, Fig.15). According to Fig.15 the sabo works can reduce the hazard and exposure of the large-scale landslide as well as the risk.

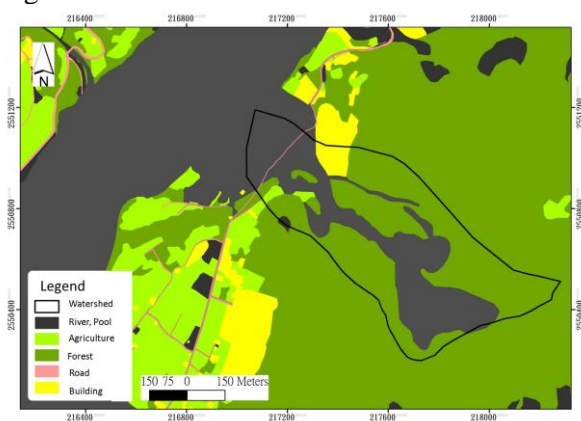


Fig 12. Risk map of Xinkai land use in 2011

4.3 Effect of sabo works

One of the objectives of this study was to propose an approach that can be used to (1) assess the risk of large-scale landslides, (2) effectively compare the risk of large-scale landslides before and after the construction of soil and water conservation

facilities, and (3) provide relevant government agencies with a reference that can benefit soil and water conservation projects. an assessment of risks related to large-scale landslides is applied after soil and water conservation facilities (Fig.14) that had been constructed in response to a large-scale landslide that took place in Xinkai.

Four sabo dams were constructed in a stream located in Xinkai Village. The heights of dams (from upstream to downstream) were 35 m, 30 m, 30 m, and 25 m, respectively, and the locations of these dams are shown in Fig.14. According to our results (Fig.14), the range of landslide deposits after building the sabo dams should be smaller than that in Fig. 11, as should deposition depth and landslide velocity. The forest land in the transportation zone is still considered to be at low risk, and the primary land used for buildings at the valley mouth is considered to be at moderate or low risk rather than high risk. The agricultural land near the edge of the alluvial fan is not within the scope of influence and not at risk.

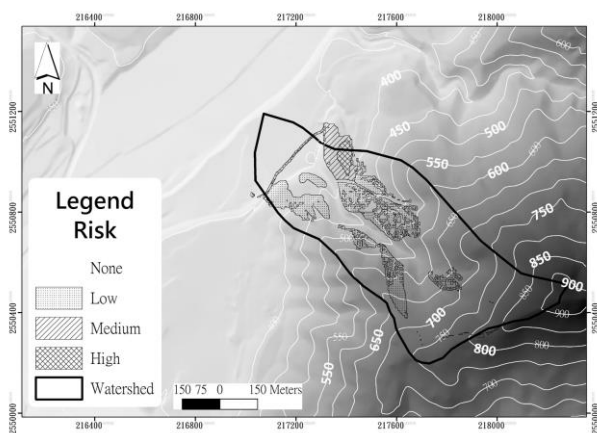


Fig 13. Risk map of Xinkai in 2011

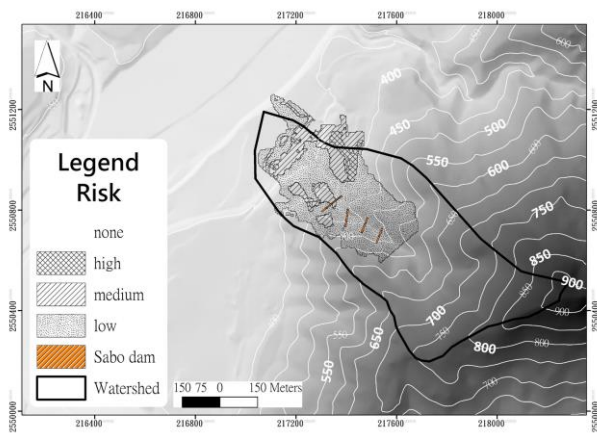


Fig 14. Location of sabo dams in upstream and risk map after completion of sabo works

5. CONCLUSION

The proposal of this study is presenting an approach can evaluate the risk of Large-scale landslide. The presented approach can not only rank the risk for each potential large-scale landslide but also can identify risk distribution in a regional area. In this research we apply the risk index approach, which can help to understand the contribution of hazard, vulnerability and exposure to overall risk is used to evaluate the risk of Large-scale landslide.

Furthermore, this approach considers the effect of mitigation work such as land-use management and sabo work. The result shows that, the potential loss can be well quantify with the approach. Furthermore, the effect of the mitigation work, such as land use managements and sabo works, can be also well described in this approach.

ACKNOWLEDGMENT: We thank the Soil and Water Conservation Bureau of the Council of Agriculture under the Executive Yuan for providing information regarding the Development and Application of Disaster Prevention and Mitigation Technologies for Large-scale Landslides project.

REFERENCES

- Australian geomechanics society (AGS), Landslide Risk Management Concept and Guidelines, Australian Geo.
- B.Yin Liu, Y.L Siu, Gordon Mitchell, Wei Xu (2016) The danger of mapping risk from multiple natural hazards. *Natural Hazards*, 82(1)
- Egashira S, Miyamoto K, Itoh T (1997) Constitutive equations of debris flow and their applicability, *Debris-flow hazards Mitigation. Water Resources Eng Div/ASCE*, pp 340-349
- Miyamoto K (2002) Two-dimensional numerical simulation of landslide mass movement. *J Jpn Soc Eros Control Eng* 55(2):5-13 (in Japanese)
- W.C Lo, T.C. Tsao, C.H. Hsu (2012) Building vulnerability to debris flows in Taiwan: a preliminary study, *Natural Hazards*, Volume 64, Issue 3, pp 2107-2128.
- Yu-Shu Kuo, Yuan-Jung Tsai, Yu-Shiu Chen, Chjeng-Lun Shieh, Kuniaki Miyamoto, Takahiro Itoh (2013) Movement of deep-seated rainfall-induced landslide at Hsiaolin Village during Typhoon Morakot, *Landslides* 10, 191-202 DOI 10.1007/s10346-012-0315-y